AD-A276 905

94-07831

A Tandem Microscopic-Electrochemical Examination of

A Charge-Induced Surface Phase Sequence:

Ordered Au(110) in Aqueous Iodide Electrolytes

as Probed by Potentiodynamic Scanning Tunneling Microscopy

DTIC
ELECTE
MAR 1 0 1994
S D
F

by

Xiaoping Gao, Gregory J. Edens, and Michael J. Weaver

Prepared for Publication

in

Journal of Physical Chemistry

Department of Chemistry

Purdue University

West Lafayette, Indiana 47907-1393

February 1994

94 3 9 075

ABSTRACT

Atomic-level structural and dynamical aspects of the electrode potential-induced sequence of surface phases on ordered Au(110) in dilute aqueous alkali iodide electrolytes have been explored by scanning tunneling microscopy (STM) coupled with cyclic voltammetry. This system exhibits a potentially rich series of electroinduced phase transitions triggered primarily by increasing iodide adsorption towards more positive potentials, together with alkali cation coadsorption. Exploration of the real-space phase-transition dynamics, in particular, is facilitated by means of "potentiodynamic" STM image sequences obtained during potential steps or especially voltammetric sweeps, thereby providing a direct link to conventional (macroscopic) electrochemical phenomena. At the most negative potentials, beyond ca -0.7 V vs SCE, Au(110) forms a largely uniform (1×3) phase. The microscopic steps associated with the formation and iodide adsorbate-induced removal of this reconstruction were examined by potentiodynamic STM. In cesium iodide electrolyte, "one-missing-row" (1×3) and (1×2) regions are seen to be formed by periodic row displacement en route to the final "three-missing-row" (1×3) phase. At higher electrode potentials, formation of a stable (1×1) substrate phase is triggered by disordered iodide adsorption. Above about -0.6 V vs SCE, several ordered iodide phases were detected. At the lowest potentials, a mixed Cs^+-I^- (2×4) adlayer was observed by STM, suggested to have the stoichiometry CsI_2. While this phase is sharply (and reversibly) removed above -0.4 V, a pair of cation-independent ordered iodide adlayers were discerned between about -0.35 and 0.2 V. The first consists of a noncommensurate near-hexagonal phase, with one iodine row rotated slightly from the $(1\bar{1}0)$ perpendicular direction. This corrugated compressible structure ("adlayer I") transforms sharply above ca 0 V vs SCE to a slightly higher-coverage, approximately (3×2) ($\theta_I = 0.67$), form ("adlayer II") with iodine rows wedged in between the $(1\bar{1}0)$ substrate "rails." The potential-induced adlayer I $\rightarrow$ II transition occurs less readily than the reverse transformation. Above 0.2 V, an unusual long-range, yet ordered, Au(110) restructuring develops featuring substrate fracturing into parallel alternating strings and ditches ca 25–40 Å wide along the $(1\bar{1}0)$ direction, but with retention of the original (1×1) substrate unit cell.

Understanding the nature of ionic adsorption on metal electrodes has long formed a central component of studies of the electrochemical double layer. The traditional double-layer structural models evolved largely from thermodynamic adsorption measurements undertaken at mercury-aqueous interfaces.[1] A longstanding issue in electrochemistry, however, concerns the extent to which the occurrence of stronger surface-adsorbate interactions expected at many solid metal surfaces, leading inevitably to larger adsorbate coverages and consequently a higher degree of adsorbate ordering, might enrich or perhaps modify this classical picture of double-layer structure. Recent innovations in experimental methodology are generating a notable renaissance of interest in such questions. Procedures for preparing and characterizing ordered single-crystal metal surfaces, once the exclusive domain of ultrahigh vacuum (uhv) surface science, have evolved recently so to encompass electrochemical systems in "in-situ" as well as "ex-situ" environments.[2,3] Of the expanding range of atomic-level techniques applicable to such in-situ electrochemical interfaces that have been developed lately, particularly noteworthy are scanning tunneling microscopy (STM) and surface X-ray scattering (SXRS).[3] While their scope is limited by various factors, in suitable cases either or both these techniques can yield remarkably detailed information on the atomic-level and nanoscale structure of ordered metal-solution interfaces.

While an emphasis has been placed so far on examining the structure of the metal substrate or metallic adlayers, both STM and SXRS are applicable to nonmetallic adsorbates, including inorganic anions. Systems studied so far include halides and sulfate on Au(111) and Pt(111),[4-8] and CO and cyanide on Pt(111) and Rh(111)[9-12] by STM, and halides on Au(111) by SXRS.[13,14] For several of these systems, especially anion adsorption on gold, the adsorbate-surface binding energy varies over the available electrode potential range sufficiently

to yield surface coverages that span the full spectrum from near-zero to saturation values. While the coverage-potential profiles can be nearly continuous throughout this range, both the in-situ STM and SXRS data display potential-induced transitions from disordered adsorption to an ordered adlayer, leading both to compressible adlayer phases and further phase transitions at high coverages.[4-7,13] A related phenomenon, also amenable to study by both STM and SXRS, concerns the removal of substrate reconstruction by anion adsorption, which can also yield sharp, although less reversible, potential-induced phase transitions.[15-17] Overall, elucidating the structural and dynamical factors that control the potential-dependent adsorbate-substrate order in such chemisorbate systems constitutes an intriguing new aspect of electrochemical surface science.[3,18]

Along these lines, we have selected for detailed study the adsorption of iodide on the three low-index faces of gold in aqueous solution by means of in-situ STM combined with conventional electrochemical methods. The value of the electrochemical techniques, while often overlooked by practioners of neoteric microscopic-level methods, lies in the opportunities for linking the atomic-level insight offered by the latter with the more "macroscopic" surface electronic and compositional information provided by the former approaches. This coupling is particularly direct (and therefore useful) under so-called "potentiodynamic STM" conditions,[5,17-19] involving the acquisition of sequences of STM images during (or between) electrochemical perturbations such as potential sweeps or steps.

We describe herein the application of potentiodynamic STM in tandem with electrochemical information, as supplied most readily by cyclic voltammetry to explore the potential-induced structural transitions associated with iodide adsorption on Au(110). This surface is of interest for several reasons, including the marked reconstruction observed at negative electronic charges which

can be lifted by anion adsorption,[16,20,21] and its "corrugated-railed" atomic morphology which may hinder hexagonal packing of adsorbate atoms. In addition, a study of the Au(110)-I⁻ system by using SXRS has been undertaken recently by the Brookhaven group.[22] The present results reveal an especially rich sequence of potential-induced phase transitions, involving striking variations in the adlayer/substrate structure and conversion dynamics. A related description of the Au(100)-I⁻ system, along with a comparison with the behavior of the other two low-index gold surfaces, is available in the following article.[23]

EXPERIMENTAL SECTION

The experimental STM procedures are largely as described in earlier reports.[5,19] The microscope is a Nanoscope II (Digital Instruments) equipped with a bipotentiostat for electrochemical STM. The STM tips were 0.01 inch tungsten wires etched electrochemically in 1 M KOH, and insulated with either clear nail varnish or a thermosetting polyethylene plastic. Most STM images were obtained in the so-called "height mode" (i.e., at constant current). The Au(110) surface (hemisphere, 5 mm diameter) was prepared at LEI-CNRS, Meudon, France, by Dr. A. Hamelin. It was pretreated by flame annealing and cooled partly in air and then in ultrapure water immediately before transferring to the STM (or conventional electrochemical) cell.[19] The counter electrode was a gold wire, and the quasi-reference electrode was a platinum wire. All electrode potentials quoted here, however, are converted to the saturated calomel electrode (SCE) scale.

The cyclic voltammetric data shown here were obtained in a conventional electrochemical cell. Additional ac impedance measurements employed a 10 mV ac signal (20 to 400 Hz) with phase-sensitive detection using a PAR Model 5204 lock-in amplifier, along with a PAR 173/179 potentiostat. All water was purified by

means of a "Milli-Q Plus" system (Millipore). All chemicals used here were reagent grade or better.

RESULTS AND DISCUSSION

A notable feature of the present Au(110)-iodide system is the occurrence of a number of (at least eight) distinct adlayer-substrate phases (or microstructures) observed by STM upon altering the electrode potential and/or the electrolyte alkali cation. As a starting point, it is instructive to consider cyclic voltammograms for this system, obtained under conditions that correspond at least partly to the STM data that follows. Figure 1A and B shows a pair of such cyclic voltammograms, obtained at 50 mV s^{-1} in 45 mM MClO$_4$ + 5 mM MI, where M - K$^+$ or Cs$^+$, respectively. The pH was adjusted to 10, so to shift the onset of hydrogen evolution beyond ca -1.0 V and thereby enable the initial stages of potential-induced iodide adsorption to be discerned more clearly.

In both electrolytes, a number of current-potential (i-E) features are observed, all of which are influenced by the presence of adsorbed iodide, and some of which are dependent also upon the nature of the electrolyte cation. It should be noted that faradaic currents are largely absent within the potential region, ca -1.0 V to 0.3 V, explored in Fig. 1, so that the i-E characteristics arise from formally *nonfaradaic* processes associated with adsorption-desorption and other surface structural transitions. As a consequence, the charge contained under most of the voltammetric features in Fig. 1A and B is largely independent of the sweep rate. (While we have selected a specific iodide concentration, 5 mM, alterations at least within the range 1-50 mM have little influence on the morphology of the voltammograms, nor does the presence or absence of the perchlorate "supporting electrolyte".) For convenience, we have labelled the most significant i-E features seen during the positive-going potential sweep as

a-g, with their identified partners observed during the reverse sweep indicated as a'-g'. While it is difficult (if not impossible) to ascertain the nature of most of the transitions by electrochemical methods alone, when coupled with potentiodynamic STM data a detailed atomic-level picture of the structure and dynamics of the transformations involved is unfolded. Rather than present STM data corresponding to a-g in alphabetical order, we consider first the region e-g where the observed phenomena are apparently dominated by substrate-iodide binding, followed by a discussion of the cation-sensitive phase transitions which occur at lower potentials.

Potential-Induced Formation of Ordered Iodide Adlayers

As in our earlier study of iodide on Au(111),[3,5,19] there is a well-defined potential region within which anion adsorption is known to be extensive, and yet where atomic-resolution images of the Au(110)-(1 × 1) substrate are reproducibly obtained. In the present case, this region contains the segment bounded by the sharp peak d/d' and the smaller feature e/e' (Fig. 1). Note that both these transitions are essentially reversible in that the positive- and negative-going partner peaks occur at virtually the same potential. (The cation-sensitive potential region below d/d' will be considered below.) Figure 2 shows an atomic-resolution STM image of a ca 160 Å square region of Au(110) containing a uniform substrate terrace, in contact with 10 mM KI. The data were obtained by rastering the tip upward within the imaged area shown, with the substrate electrode potential held initially at -0.35 V (i.e. between d and e), and then stepped to -0.2 V (i.e. between e and f) about halfway along the image acquisition.

Evident in the lower portion of this "composite-domain" image in Fig. 2 (i.e. at -0.35 V) is a pattern consistent with an ordered Au(110)-(1 × 1) substrate, featuring bright dots (i.e. tunneling maxima) forming parallel rows

4.1 (± 0.1) Å apart, each dot being separated by 2.9(± 0.05) Å. In K^+ (or Na^+)-based electrolytes, such ordered (1 × 1) substrate images are also evident at potentials below d/d′, down to ca -0.6 V, although different behavior is seen in CsI electrolyte (vide infra). The upper portion of Fig. 2, however, contains a markedly different imaged pattern, consistent with the presence of an ordered iodide (or monoatomic iodine[24]) adlayer. The potential-induced formation (or removal) of the ordered adlayer is indeed responsible for the e/e′ voltammetric feature, as discerned from STM images acquired during small potential steps in this region. Another image of the adlayer structure at -0.1 V, showing clear corrugation patterns, is shown in Fig. 3A; a height-shaded close-up of part of the imaged region is displayed in Fig. 3B.

Such images enable a surprisingly accurate as well as detailed determination of the iodine adlayer structure to be made, including the registry with the substrate adlattice. As outlined previously,[5,18] "composite-domain" images such as Fig. 2 allow the spatial relationship between the substrate and adlayer atomic lattices to be deduced by mutual extrapolation of the patterns within regions close to the electrochemically induced real-space domain edge. Another important virtue of this procedure is that it can circumvent the deleterious effects of thermal (and other instrument) drift in STM which can skew both the apparent interatomic distances and row angles, i.e. x-y distortion.[5,18] [An example of the latter artifact is perceptible at the bottom of Fig. 2, where the Au(110) top-layer gold rows appear to "bend" significantly.] Since the substrate lattice parameters are known independently (and very accurately), the substrate lattice region adjacent to the adlayer domain can be employed as an "internal calibration."

An additional means of determining the adlayer structure, clearly observable in the present case, concerns the ordered periodic variation in the

"brightness" (i.e. the z-displacement) along and across the iodine rows. At least for simple adsorbates, such as iodine, the z-displacement observed in the STM images can be identified at least roughly with the actual differences in the z-position associated with different binding sites.[5,8,18] Thus iodine atoms adsorbed in atop sites usually appear "brighter" than those coordinated in doubly bridging or especially in threefold or fourfold hollow sites. This point can be confirmed for the present adlayer structure by inspecting the juxtaposed adlayer/substrate region in Fig. 2: adlayer atoms lying along an extension of the (110) substrate "rails" appear brighter than those located between the gold rows. Indeed, these periodic corrugation (or "moiré") patterns provide an additional means of ascertaining the adlayer-substrate atomic registry as well as yielding an accurate real-space adlayer structure.

A ball-model representation of the iodine adlayer pattern corresponding to Figs. 2 and 3 is provided in Fig. 4A. [In actuality, Fig. 4 shows the mirror-image (rotational domain) structure to that seen in Fig. 2 and 3; nevertheless, both rotational domains were commonly observed, occasionally appearing together on the same substrate terrace region.) The unit cell of this structure (dubbed here "adlayer I"), having the approximate symmetry ($\sqrt{11} \times 13\sqrt{2}$) or more properly ($\begin{smallmatrix} 0 & 13 \\ -3 & 1 \end{smallmatrix}$), is complex. It involves a 4° rotation of one iodine row on the near-hexagonal adlattice away from the (100) substrate direction (i.e. perpendicular to the gold atomic rails). The iodine-iodine interatomic spacing, d_{I-I}, is about 4.4 Å along these rows (i.e. approaching the van der Waals iodine diameter, 4.3 Å), and rather longer, ca 4.8 Å, along the other two row directions, running more diagonally across the substrate top-layer "rails."

At potentials close to e/e', the adlayer coverage, θ_I, is about 0.62. Increasing the electrode potential towards the next voltammetric feature, f/f', occurring at about 0 V, yields a small yet significant compression of the adlayer

involving a further diminution of the d_{I-I} value along the near-(100) direction down to about 4.3 Å together with some decrease in the spacing along the other two row directions. These variations can be seen most readily by examining STM images acquired during suitable potential-step perturbations. The segments of "bright" iodine atoms seen along the near-(100) rows, corresponding to several adjacent iodines bound in near-atop sites, are seen to lengthen, with a corresponding expansion of the unit cell. The overall coverage increase induced by this distortion, however, is only small, 0.02-0.03. Note that the Au-Au spacing along the (100) direction is slightly shorter (4.08 Å) than the iodine diameter; this mismatch is accommodated by the observed slight rotation of the I rows.

Although the iodine adlayer commonly features large and uniform domains, some interesting irregularities can also be observed. An example is evident in Fig. 3A, and more clearly in Fig. 3B, in the form of small "holes" bounded by three or so iodine atoms on each side. Once formed along with the adlayer, they are quite stable and immobile, at least over ca 30 min or so. Aside from the interesting nature of such defects, observing such clearcut interruptions in the atomic patterns (Fig. 3B) provides assurance that *true* atomic resolution is being achieved, rather than the occurrence of repetitive patterns influenced by "blunt-" or "multiple-tip" artifacts.

Altering the potential above 0 V results in a marked change in the iodine adlayer geometry. The nature of this second, "high-potential", compressed adlayer (labelled here "adlayer II") is seen most readily by inspecting Fig. 5A. Similarly to Fig. 2, this is a composite-domain STM image obtained for Au(110) in 10 mM KI by stepping the electrode potential during the upward-rastered data acquisition. Now, however, the potential was altered from a value (-0.45 V) where the (110) substrate is seen, to a point (in this case 0.1 V) suitably

beyond the voltammetric feature f. While some image instability is evident, generated partly by the large potential step, a markedly different near-hexagonal iodine adlayer pattern is seen that includes iodine rows running parallel to the $(1\bar{1}0)$ direction, and located in between each top-layer gold atomic row.

We have described briefly this adlayer structure in an earlier survey.[18] A ball-model representation of the approximately (3 × 2) unit cell of adlayer II is shown in Fig. 4B. Note the predicted presence of alternating twofold and fourfold hollow binding sites along the $(1\bar{1}0)$ substrate direction. Little or no difference in z-displacement is seen between iodines bound at these two types of multifold sites, hampering somewhat the estimation of accurate coverages directly from the STM patterns. [This situation is similar to that encountered for the approximately (5 × √3) structure observed for the Au(111)-I system.[5,25]] Nevertheless, the c(3 × 2) structure shown in Fig. 4B corresponds to θ_I - 0.67, with a d_{I-I} distance along the $(1\bar{1}0)$ direction of 4.35 Å, and a diagonal d_{I-I} value of 4.6 Å. Increasing the potential to higher values yields slight compression along the $(1\bar{1}0)$ direction, but other more significant microstructural changes also set in under these conditions, as described below.

While the average coverage of adlayer II is only slightly (0.02-0.03) higher than can be attained for the lower-potential "corrugated" adlayer I, it is clear that marked changes in the iodine atomic packing arrangement are required in order to transform adlayer I to II. The significant hysteresis observed between the positive- and negative-going voltammetric features f and f' indicates that the adlayer I ↔ II phase transition involves a degree of electrochemical irreversibility. Some intriguing information on the *microscopic* phase-transition dynamics associated with the potential-induced I ↔ II conversion was obtained from composite-domain STM images generated by either potential steps or sweeps across the potential region, roughly -0.1 to 0.1 V, where the

transition occurs. Figure 5B shows such an image obtained by stepping the potential from about -0.05 V to 0.05 V about halfway along the upward-rastered data acquisition. An essentially discontinuous phase change (< 0.1 s) from a uniform adlayer I to II is seen to be achieved under these conditions.

Markedly different behavior is observed, however, during a similar potential excursion, but now using a relatively slow (5 mV s^{-1}) potential *sweep*. Figure 5C displays such an image, again obtained in an upward-rastered fashion, from about -0.02 to 0.05 V (the data acquisition time is 15 s). Note that the y-axis in this case can also be regarded as a linear scale of potential and time, both increasing in the upward direction, so that imaged regions lying along a line paralleling the x-axis correspond to the same potential and time [cf ref. 19]. About two-thirds along the image acquisition, the previously uniform phase I is seen to commence conversion to phase II. However, while this transformation is evident towards the top right-hand side of the imaged area, the corresponding left-hand region displays local disorder, and only achieves complete conversion to structure II just beyond the end of the image acquisition. The phase transition, therefore, does not occur in a strictly discontinuous fashion, but rather over a significant, ca 25 mV, potential span.

Undertaking the reverse potential-induced phase change, II → I, yields a somewhat sharper transition, as exemplified in Fig. 5D. This image was obtained shortly after Fig. 5C, but now for a negative-going 5 mV s^{-1} potential sweep from 0 to -0.08 V during the downward-rastered data acquisition. Evident is a clearcut phase transition from adlayer II to I occurring towards the bottom of the image, at about -0.05 V. The transformation is seen to be complete within a narrow potential span, only about 5 mV.

It is of particular interest to compare such inherently atomic-scale (microscopic) insight into the phase-transition dynamics with the *macroscale*

information available from corresponding cyclic voltammograms. For this purpose, the inset C in Fig. 1 contains a pair of cyclic voltammograms recorded at 5 (lower) and 50 mV s^{-1} (upper), with the potential excursion restricted to the narrow potential region -0.1 V to 0.05 V that just encompasses the transition f/f'. [The current (y-axis) scale for the former is magnified by 10-fold so to compensate for the slower sweep rate.] The conditions used for the 5 mV s^{-1} voltammogram match closely those for the potentiodynamic STM data in Figs. 5C and D, and are free of the complications that ensue when wider potential excursions are employed (vide infra). The magnitude as well as sign of the (essentially constant) charge contained under the voltammetric peaks f and f' is approximately consistent with the microscopic phase change given that the adlayer conversion I → II involves a slight yet significant coverage change, yielding a nonfaradaic charge "pulse" associated with iodide surface binding. As might be expected, decreasing the voltammetric sweep rate yields a diminution in the potential peak separation between f and f'. Particularly evident at 5 mV s^{-1} is a "sharpening" of peak f'. Comparison with the corresponding STM images (Figs. 5C and D) indicates that the breadth of the positive-going voltammetric peak f matches well with the microscopic data in that both indicate a "transition width", ΔE_t, of 25-30 mV. However, the return voltammetric peak f', although narrower than f, is significantly broader than the ΔE_t value, $\leq$ 5 mV observed in the STM images. This finding may implicate an interesting distinction between "microscopic" and "macroscopic" phase transitions (vide infra).

Beyond the transition f/f' is located another somewhat irreversible feature g/g', with the positive-going peak (g) centered at about 0.07 V, with the return wave (g') at 0 V (Fig. 1A, B). Either holding or sweeping the potential beyond ca 0.1 V yielded not only a growth in g' but also a commensurate distortion in f'. The microscopic nature of this g/g' transition is not entirely clear.

Nonetheless, STM images obtained under similar conditions, especially holding the potential in the range 0.1–0.25 V for 1–2 min., indicated the apparent formation of iodine strings imbedded into the (3 × 2) adlayer. These strings are evident in the large–scale image shown in Fig. 6A: the bright "ad–rows" are seen to run along directions rotated about 30° from the (110) substrate "rails." A close–up (atomic–resolution) image of a trio of such strings overlaid on the (3 × 2)–I adlattice is shown in Fig. 6B.

Positive Potential–Induced Nanoscale Structural Changes in Substrate

Although we have focussed so far on atomic structural changes associated with ordered iodine adlayers, there are two significant alterations evident in the nanoscale substrate morphology that are seen to occur upon adjusting the potential to values, above ca –0.3 V, where the ordered iodine adlayers are present. The first type of morphology change concerns the form of the terrace edges. Figures 7A and B show similar large–scale (200–250 nm) regions of the Au(110) surface in 10 mM KI, obtained at –0.4 V and ca 2 min. after increasing the potential to 0.1 V. The former image shows several terrace edges, the directions of which appear rounded, even semicircular. Such terrace–edge patterns are commonly seen on Au(110) and other low–index gold surfaces, and probably arise from the need to minimize the proliferation of the terrace edges (i.e. step sites) in comparison with the flat terrace regions. The higher–potential image (Fig. 7B), however, exhibits markedly straighter terrace edges that change direction abruptly, rather than displaying sweeping curves. Interestingly, the terrace–edge directions are consistently rotated about 30° from the (1$\bar{1}$0) direction, i.e. lying roughly along the same direction as the iodine "ad–rows" noted in Fig. 6A. (Indeed, a similar terrace–edge morphology, as in Fig. 7B, is also evident in Fig. 6A.) This structural change occurs at

potentials above -0.3 V, and quite rapidly (within 1-2 min.) above 0 V. Evidently, then, the presence of the ordered iodine adlayers, especially the close-packed (3 × 2) adlattice, can exert a marked influence on the terrace-edge superstructure.

The second, and especially intriguing, nanoscale structural change appears upon holding the electrode potential at slightly higher values, in the region 0.3-0.4 V. (Note that solution-phase iodide electrooxidation to form iodine multilayers commences only at about 0.45 V.) While the nature of the periodic substrate restructuring that occurs under these conditions is detailed elsewhere,[26] we provide a brief description here for convenience. Figure 7C shows a large-scale region of Au(110) in 10 mM KI containing a number of separate terraces a few minutes after increasing the potential to 0.25 V. The inward- and outward-jutting terrace corners, seen already for another surface region in Fig. 7B, have become decidedly indented and protruded, respectively, along with the appearance of iodine strings, already noted in Fig. 6. An increasingly marked and uniform restructuring occurs upon holding the potential at 0.25-0.4 V for longer periods, the changes occurring more rapidly at higher potentials. Figure 7D shows the same imaged region as in Fig. 7C, but after holding at 0.35 V for 15 min. Clearly evident are near-parallel alternating strings and ditches, spaced about 25-30 Å apart, which meander close to the $(1\bar{1}0)$ direction. This pattern is seen to result from a remarkably extensive and concerted motion of gold atoms by development of the indentations and protrusions in Fig. 7C, so that the formerly distinct terrace regions have now largely merged in Fig. 7D. The channels typically involve one-atom corrugations across the rows, although double steps can be seen in regions formerly close to terrace edges. An atomic-resolution closeup of a typical restructured region is shown in Fig. 7E. The continued presence of the (3 × 2) adlayer pattern can be discerned, so that the

restructuring involves *only* the production of longer-range (20-40 Å) periodicities in the form of the step edges running preferentially in the (1$\bar{1}$0) direction. Notably, these structural changes can largely be reversed within a few minutes by lowering the potential below 0.2 V or so.

A discussion of the likely factors responsible for this remarkable long-range restructuring is given in ref. 26. Briefly, a simple physical model invokes a destabilization of the two-dimensional terraces by dipole-dipole repulsion between nearby sites involving the close-packed adsorbed iodide. The significant point is that such dipole-dipole arrays feature relatively long-range interactions which will destabilize sites in uniform terrace regions relative to those near terrace edges. Cleaving the top-layer surface periodically along the (1$\bar{1}$0) direction, as in Fig. 7D, should have the effect of diminishing the adlayer repulsion energy, at the expense of creating more terrace-edge sites. The latter energy cost is expected to be relatively *small given the large distance (ca 4.1 Å) between adjacent (110) top-layer rows*. The sensitivity of the occurrence of the long-range restructuring to the electrode potential may be rationalized on the basis of the increasing positive electrode charge, and hence larger effective adsorbate-surface moment, present under these conditions.[26]

While a chemically distinct phenomenon, it is also appropriate to comment here on the nature of the polyiodine multilayer films that are generated by the onset of solution iodide electrooxidation at $\geq$ 0.45 V. We have noted the variety of multilayer polyiodine film structures created in this fashion on Au(111).[5] Figure 7F displays a Au(110) surface region imaged after initiating a controlled amount of iodide electrooxidation close to 0.45 V. The bottom one-third shows a preponderance of the restructured strings/channels just noted, covered with a (3 × 2) iodine adlayer. Elsewhere in the image, however, quite different atomic patterns can be discerned, arising evidently from polyiodine formation.

Significantly, the film structure is at least partly in registry with the substrate in that the distance across the "square-planar" packed blocks is twice that across the (110) rails, about 8.2 Å. Several other distinct polyiodine structures can commonly also be observed, depending on the film formation conditions [cf the Au(111)-I system].[5]

Negative Potential-Induced Au(110) Reconstruction

While the Au(110) substrate restructuring just described, occurring at higher positive potentials, has not apparently been observed previously, a now well-documented phenomenon is the occurrence of Au(110) reconstruction at negative electrode charges.[16,20,21] Similarly to this and other (110) surfaces in uhv,[27] a "missing-row" type of reconstruction is observed in aqueous electrochemical environments.[16,20,21] While a (1 × 2) symmetry is often observed in non- (or weakly-) adsorbing electrolytes,[20,21] Ocko et al have shown from SXRS measurements that at sufficiently negative potentials a (1 × 3) reconstruction predominates.[16] Given that adsorbed iodide lifts the reconstruction over most of the electrode potential range considered here, it is of some interest to examine STM images at sufficiently negative potentials where iodide is sufficiently desorbed to engender Au(110) reconstruction. From other studies,[3,17,23] the pronounced voltammetric features b and b' seen in Fig. 1A are anticipated to indicate the removal and formation, respectively, of the reconstruction. Of particular interest is the marked difference in the form of the b/b' transition in KI and CsI electrolyte (Fig. 1A, B). This observation clearly signals a role of cation adsorption (or cation/anion coadsorption) in the reconstruction process. A fuller discussion of the microscopic phenomena involved will be available elsewhere,[28] so that the presentation of the STM data here will be brief.

A sequence of four potentiodynamic STM images, obtained for Au(110) in 10 mM KI during a 10 mV s⁻¹ potential excursion from ca -0.45 V to -0.8 V and return, are shown in Fig. 8A-D. The first, upward-rastered, image (A) was acquired while the potential was swept from -0.6 to -0.8 V. Just prior to this image [and again upon completion of the voltammetric cycle (Fig. 8D)], a semicircular series of terrace edges (convex to the top horizontal axis) were present. While vestiges of the smooth terrace edges are discernable at the bottom of Fig. 8A, by about one-third up the image (i.e. by about -0.67 V), densely packed corrugated strings along the (1$\bar{1}$0) direction become predominant. These strands act to blur the original terrace-edge positions in that extended kinks are formed. The production of the reconstructed strings is essentially complete on this timescale by about -0.7 to -0.75 V.

This potential-induced phase transition matches well the location of peak b' in Fig. 1A, bearing in mind that this feature is shifted about 0.05 V positive at the slower (10 mV s⁻¹) sweep rate used for the STM data acquisition. The reconstruction is seen to be present uniformly throughout the same examined area in the subsequent downward-rastered STM image (Fig. 8B), obtained while the potential was swept from -0.8 V to -0.84 V and back to -0.68 V. The unit-cell symmetry is mostly (1 × 3) (i.e. the parallel strings, or tunneling maxima, being separated by 12.2 Å), but with some local regions featuring larger string separations [i.e. (1 × n), where n > 3] or having (1 × 2) symmetry. Traversing the potential back to less negative values through the voltammetric feature b (Fig. 1A) yielded complete removal of the reconstruction, at about -0.55 to -0.6 V. This is seen clearly in the next, upward-rastered, image (Fig. 8C), referring to the potential span -0.68 V to -0.48 V. Immediately upon reaching the return potential, -0.45 V, a completely (1 × 1) surface is recovered (Fig. 8D). This features terrace-edge morphologies that are not greatly different from those

observed prior to the potential cycle.

As already mentioned, the voltammetric data in CsI electrolyte shows a markedly different morphology in the b/b' region in that a readily distinguishable pair of peaks, labelled b_1/b_1' and b_2/b_2' were obtained (Fig. 1B). Potentiodynamic STM experiments were therefore also undertaken in CsI media to ascertain if these electrochemical differences could be identified with clearcut microscopic structural effects. Figure 9A shows a large-scale upward-rastered image dominated by one large terrace for Au(110) in 10 mM CsI, obtained while the potential is swept negative from -0.55 to -0.65 V at 5 mV s^{-1}. Towards the top of the image, and especially close to the terrace edges, a (1 x 3) reconstruction becomes evident. The next downward-rastered image (Fig. 9B), was obtained during the ensuing potential-sweep segment from -0.65 to -0.75 V. This potential sector corresponds to the voltammetric region between b_2' and b_1' at the 5 mV s^{-1} sweep-rate employed. Evident in Fig. 9B is a uniform (1 x 3) reconstruction pattern throughout the terraces, of the type seen to be initiated in the upper region of the preceding image (A).

Detailed examination of the reconstruction profile from the STM images, however, indicates that the form of this (1 x 3) reconstruction is quite different from the type seen to be generated in the KI electrolyte (Fig. 8B). The latter features a symmetric "v-shaped" z-x profile across the ($1\bar{1}0$) direction, with a ca 2 Å corrugation between the monoatomic rails. This (1 x 3) structure is commonly observed in (or inferred from) measurements of (110) surfaces in uhv,[29] and has been termed a "three-missing-row" structure, denoting the (formal) loss of a trio of top-layer metal rows across each unit cell.[30] The (1 x 3) reconstruction seen in Fig. 9B, however, consists of pairs of adjacent (110) monoatomic rails, each separated by a single missing row. This latter pattern, which has been called the "one-missing-row" structure, is less commonly

observed (or predicted) in uhv (e.g. ref. 31). Interestingly, the one-third row atoms missing from the top layer are seen to be shifted so to form single- and double-atomic string segments alongside the (1 × 3) lattice: these appear as bright rows in Fig. 9B. (The bright strings are largely absent close to the terrace edges, presumably because they have been incorporated into the steps.)

Further structural changes are seen in the next, upward-rastered image (Fig. 9C), corresponding to a potential sweep from −0.75 V to −0.85 V (i.e. straddling the voltammetric peak b_1' and an additional "satellite peak" at slightly more negative potentials). A markedly increased density of bright (adlayer) strings is evident, along with the formation of surrounding (1 × 2) corrugated regions. This conversion process continues at higher potentials, at −0.85 to −0.95 V, until a nearly uniform array of the adlayer strings is formed, now having (1 × 3) symmetry of "the three-missing-row" type. This final reconstructed form, similar to that produced in KI electrolytes (Fig. 8B), is shown in Fig. 9D.

The significance of this finding in the present context, then, is that the multiple-peaked voltammetric response obtained during the formation of the symmetric (1 × 3) reconstruction in CsI electrolyte can be identified clearly as occurring in spatially as well as potentiodynamically distinct stages. In a broader perspective, the clearly observed fate of the missing-row atoms in the intermediate (1 × 3) [and (1 × 2)] structures, seen in Fig. 9B and C, is apparently unprecedented in studies of such (110) and related reconstructions. These separate steps may also occur in KI electrolyte, as indeed suggested by the twin-peaked form of b' in Fig. 1A, but cannot clearly be spatially or temporally resolved at the microscopic level in this case. While the role of adsorbed cesium in influencing the reconstruction process is not yet clear, this phenomenon may well be related to the observation of (1 × 3) reconstruction of

Au(110) induced by Cs (and other alkali metals) in uhv.[32]

Ordered Cesium/Iodide Adlayers

As already mentioned, sweeping the potential positive of the voltammetric feature b (or b_2) (Fig. 1) yields a sharp removal of the substrate reconstruction, leaving well-ordered Au(110)-(1 × 1) terraces. Such terraces are also evident in STM images obtained in KI electrolytes over the potential region up to the formation of the ordered iodide type I adlayer denoted by e/e' in Fig. 1. In recent SXRS experiments undertaken on the present system, however, Wang and Ocko observed the formation of a coadsorbed K/I adlayer within the potential region that encompasses the voltammetric features c/c' and d/d'. An apparently similar ordered adlayer was observed in that study in CsI electrolyte. Such ordered adlayers could also be discerned in KI media by STM, although not consistently at the higher tunneling currents desirable for the clearcut observation of atomic features. Images indicating their presence were nonetheless reproducibly obtained in the CsI solutions employed here.

Figure 10 A shows an atomic-resolution "composite-domain" image obtained for Au(110) in 10 mM CsI by stepping the potential from -0.3 V to -0.5 V about one-third along the upward-rastered data acquisition. While the bottom third of the image shows clearly the substrate (110)-(1 × 1) pattern, a markedly different structure prevails uniformly above this point. The adlayer pattern consists of tunneling maxima located along each (110) substrate "rail", the members of each string being separated in this direction by ca 5.8 Å, i.e. two gold atomic strings. The adlayer was observed to be stable over the potential range -0.4 V to around -0.55 to -0.6 V. The positive potential limit coincides with the reversible voltammetric peaks d_1/d_1' (Fig. 1B).

Related, yet significantly different, structural patterns can be obtained,

however, depending on the precise tunneling conditions, such as the sign of the tip-substrate bias combined with the electrode potential. Figures 10B and C show representative images consisting of commonly observed patterns. The former displays strings along the (110) direction of the type seen in Fig. 10A, again spaced two gold atoms apart, but now alternating with rows having weaker tunneling maxima but with a twofold higher density, i.e. spaced only 2.9 Å apart. A closely related pattern is evident in Fig. 10C, the difference with Fig. 10B being the clearer occurrence of a "zig-zag" atomic arrangement along the more weakly imaged rows, so to yield an essentially hexagonal adlayer pattern.

While the tunneling-dependent variations in the imaged patterns clearly complicate attempts to assign real-space structures, one has some confidence in the likely validity of the higher adlayer coverage inferred from Fig. 10C, given that the occurrence of inferior spatial resolution can readily account for the simpler pattern seen in Fig. 10A. A plausible real-space adlayer structure, derived from images such as Fig. 10C, is shown in ball-model form in Fig. 10D. We assign the "brighter" spots, lying at the corners of the (2 × 4) unit cell as shown, to cesium adatoms (or ions) bound to bridging sites along the (110) substrate rails. The "weaker" spots forming the staggered alternate rows are assigned to adsorbed iodide bound sites having almost fourfold-hollow symmetry (Fig. 10D). The total adlayer coverage in this (2 × 4) patterns is 0.75, with a 2:1 ratio of iodine to cesium atoms.

Such an adlayer structural assignment on this basis is, of course, only tentative. The implication that the cesium adatoms incur stronger tunneling maxima than adsorbed iodine is perhaps surprising, even given the expected difference in actual z-displacement arising from the distinct binding sites. A possible alternative structure can be envisaged by reversing the tunneling maxima assignments, thereby placing adsorbed iodine atoms along the substrate rails.

This arrangement would, however, invert the iodine-cesium coverage ratio, yielding a 2:1 excess of alkali metal. The former adlayer structure (shown in Fig. 10D) would appear to be more likely on electrochemical grounds, which favor an iodide-rich stoichiometry as is noted below. The total coverage observed for this mixed cation/anion adlayer by STM, θ - 0.75, along with the overall hexagonal adlayer pattern, matches that obtained by SXRS.[22]

General Discussion and Conclusions

A notable feature of the present system as revealed by STM is the diverse microscopic nature of the potential-dependent surface structures and phase transitions apparent in the cyclic voltammetry. As stated at the outset, the primary focus of this paper is to illustrate the manner and degree to which such double-layer phenomena can be usefully explored by means of tandem voltammetric and potentiodynamic STM measurements. In order to approach more closely that goal, it is appropriate to discuss in more unified terms the nature of the cyclic voltammetric response in the light of the above findings.

We have not commented up to now on the broad symmetrical feature a/a' which appears at far negative potentials (Fig. 1A, B). As delineated more readily by differential capacitance measurements,[33] this commonly observed feature arises from the initial stage of iodide adsorption in the form of a low-coverage, almost certainly disordered, phase. Additional differential capacitance-potential (C_d-E) data for Au(110) obtained from ac impedance measurements show that the negative-potential side of the broad C_d-E hump is shifted slightly (ca 50 mV) negative in the CsI compared with the KI electrolyte.[34] This indicates a degree of cation cooperatively in the initial stages of iodide adsorption, suggestive of some cation coadsorption on the (1 × 3) reconstructed surface.

The marked influence of cesium cations on both the voltammetric signature (b/b') and microscopic nature of the (1 × 3) → (1 × 1) substrate phase transition

show clearly that this phenomenon can be influenced importantly by cation as well as anion adsorption, at least in the cesium electrolyte. The magnitude of the charge contained under b/b', ca 40–50 μC cm^{-2}, suggests that the $(1 \times 3) \rightarrow (1 \times 1)$ substrate transition is accompanied by substantial increases in the iodide coverage $(\Delta \theta_I \sim 0.3)$ on the unreconstructed versus the reconstructed gold surface. The C_d–E measurements indicate that the $(1 \times 3) \rightarrow (1 \times 1)$ conversion is triggered when the iodide coverage reaches about 0.1. The broad and somewhat hysteretic nature of the b/b' voltammetric transition is also worthy of comment here. While the elementary steps involved in the $(1 \times 3) \rightarrow (1 \times 1)$ transition appear to be facile, from the potentiodynamic STM data one can conclude that the formation and removal of the reconstruction follow microscopically distinct pathways. The physically irreversible nature of the $(1 \times 3) \rightarrow (1 \times 1)$ transition is also indicated from the virtual absence of an ac impedance response, even at low ac frequencies (down to 20 Hz).[23] A similar conclusion also applies to the adsorbate–driven lifting of reconstruction at the other low–index gold surfaces.[23,34]

Once formed, the (1×1) surface in the potential region c/c' bounded by b/b' and d/d', involves ordered anion/cation coadsorption as divulged by the voltammetry, STM, and perhaps most clearly from SXRS data.[22] A conceivably related ordered phase involving anion/cation coadsorption has been proposed on the basis of STM measurements for sulfate adsorption on Au(111) at high potentials in acidic media.[7] More generally, such coadsorption has been observed in diverse other electrochemical systems.[35,36] Iodide adsorption on gold, however, is usually expected to involve substantial, even near–complete, adsorbate–surface charge transfer as indicated from electrosorption valency[37] and potential–dependent Raman spectroscopic data.[38] The occurrence of alkali cation coadsorption may be driven by a need to diminish the anion–anion inner–layer

repulsion anticipated at higher iodide coverages. While such coadsorption would appear unnecessary if the anion charged is indeed largely transferred upon adsorption, one could imagine a partially charged anion adsorbate state being stabilized in the presence of the coadsorbed cation. On this basis, however, we expect that the anion/cation stoichiometry should exceed unity, supporting the suggested coadsorbate phase structure shown in Fig. 10D. Nevertheless, the role and occurrence of cation coadsorption in ordered anion adsorbate phases is clearly an ill-understood, as well as intriguing, issue at the present time.

The sharp (and electrochemically reversible) loss of adsorbate order towards higher potentials as signalled by the transition d/d' and accompanying STM (and SXRS[22]) data is another unexpected finding. One can rationalize the removal of the coadsorbed cation as being triggered by the increasingly positive electrode charge. The reoccurrence of iodide adsorbate ordering at high potentials, above e/e' is less surprising: ordered adlayer structures are often formed with both nonmetallic and metallic adsorbates once the coverage climbs towards saturation.[3] This phenomenon is readily understandable in general terms as arising from the combined influence of strong adsorbate-adsorbate interactions and the energetic preference for specific surface binding sites. The structural and dynamical nature of the high-potential iodide adlayers on Au(110) are discussed in comparison with the corresponding Au(111) and Au(100) systems in the following article.[23] It is nonetheless worth reiterating here the value of tandem voltammetric and potentiodynamic STM measurements, as illustrated in Fig. 5B-d, for unraveling possible differences in the dynamics of surface phase transitions in a macroscopic and microscopic sense. Thus the smaller ΔE_t value extracted for the adlayer II → I conversion from STM compared with voltammetric sweep measurements suggests that the latter may reflect an averaging of arrays of phase transitions occurring on terrace domains of varying sizes and shapes,

for example, that exhibit significantly different potential-dependent equilibria and/or dynamics. At least in principle, such measurements offer a new dimension of insight into potential-induced adlayer phase transitions.

Finally, the long-range ordered substrate restructuring noted beyond g/g′ highlights further the remarkably varied influence that iodide adsorption exerts upon the Au(110) surface structure. Taken together, this system provides perhaps a benchmark example of the diverse structures that can be induced in electrochemical environments by suitable alterations in the electrode potential (and hence in electronic charge and electrostatic field strength). The richness of the phenomena involved, and the prospects for further detailed exploration of such phases by combined electrochemical and in-situ microscopic methods, suggest that our understanding of double-layer structure stands to be advanced on a distinctly broader front by tandem experiments of this type.

References and Notes

1) Delahay, P. in, "Double Layer and Electrode Kinetics", Wiley Interscience, New York, 1965.

2) For detailed recent overviews, see: (a) "Structure of Electrified Interfaces", Lipkowski, J. and Ross, P.N., eds., VCH Publishers, New York, 1993; (b) "Adsorption of Molecules at Electrodes", Lipkowski, J. and Ross, P.N., eds., VCH Publishers, New York, 1992.

3) Weaver, M.J. and Gao, X., Ann. Rev. Phys. Chem., 1993, 44, 459.

4) Tao, N.J. and Lindsay, S.M., J. Phys. Chem., 1992, 96, 5213.

5) Gao, X. and Weaver, M.J., J. Am. Chem. Soc., 1992, 114, 8545.

6) Magnussen, O.M., Hageböck, J., Hotlos, J., and Behm, R.J., Far. Disc., 1992, 94, 329.

7) Edens, G.J., Gao, X., and Weaver, M.J., J. Electroanal. Chem., submitted.

8) Yau, S-L., Vitus, C., and Schardt, B.C., J. Am. Chem. Soc., 1990, 112, 3677.

9) Yau, S-L., Gao, X., Chang, S-C., Schardt, B.C., and Weaver, M.J., J. Am. Chem. Soc., 1991, 113, 6049.

10) Oda, I., Inukai, J., and Ito, M., Chem. Phys. Lett., 1993, 203, 99.

11) Villegas, I. and Weaver, M.J., in preparation.

12) Stuhlmann, C., Villegas, I., and Weaver, M.J., Chem. Phys. Lett., in press.

13) Ocko, B.M., Watson, G.M., and Wang, J., J. Phys. Chem., 1994, 98, 897.

14) Wang, J. and Ocko, B.M., unpublished results.

15) Wang, J., Ocko, B.M., Davenport, A.J., and Isaacs, H.S., Phys. Rev. B, 1992, 46, 10321.

16) Ocko, B.M., Helgensen, G., Schardt, B.C., Wang, J., and Hamelin, A., Phys. Rev. Lett., 1992, 69, 3350.

17) Gao, X. and Weaver, M.J., J. Phys. Chem., 1993, 97, 8685.

18) Gao, X. and Weaver, M.J., Ber. Bunsenges. Phys. Chem., 1993, 97, 507.

19) (a) Gao, X., Edens, G.J., Hamelin, A., and Weaver, M.J., Surf. Sci., 1993, 296, 333; (b) Hamelin, A., Stoicoviciu, L., Edens, G.J., Gao, X., and Weaver, M.J., J. Electroanal. Chem., in press.

20) Magnussen, O.M., Wiechers, J., and Behm, R.J., Surf. Sci., 1993, 289, 139.

21) (a) Gao, X., Hamelin, A., and Weaver, M.J., Phys. Rev. B, 1991, 44, 10983; (b) Gao, X., Edens, G.J., Hamelin, A., and Weaver, M.J., Surf. Sci., submitted.

22) Ocko, B.M. and Wang, J., in preparation.

23) Gao, X., Edens, G.J., Liu, F-C., and Weaver, M.J., J. Phys. Chem. (following article).

24) We utilize the terms adsorbed iodine and iodide interchangeably here, since adsorbed iodide on gold appears to feature essentially complete charge transfer (or charge sharing) between the adsorbate and the metal surface,[5] at least in the absence of coadsorbed cations (also see text and footnote 15 of ref. 23).

25) Haiss, W., Sass, J.K., Gao, X., and Weaver, M.J., Surf. Sci., 1992, 274, L593.

26) Gao, X. and Weaver, M.J., Phys. Rev. Lett., submitted.

27) For example: Gritsch, T., Coulman, D., Behm, R.J., and Ertl, G., Surf. Sci., 1991, 257, 297.

28) Gao, X. and Weaver, M.J., Surf. Sci., submitted.

29) Robinson, I.K., Eng, P.J., Romainczyk, C., and Kern, K., Phys. Rev. B, 1993, 97, 10700, and references cited therein.

30) (a) Masson, F., and Rabalais, J.W., Surf. Sci., 1991, 253, 258; (b) Thiel, P.A. and Estrup, P.J., in "CRC Handbook of Surface Imaging and Visualization", Hubbard, A.T., ed., CRC Press, in press.

31) Schuster, R., Barth, J.V., Ertl, G., and Behm, R.J., Surf. Sci., 1991, 247, L229.

32) Häberle, P., Fenter, P., and Gustafsson, T., Phys. Rev. B, 1989, 39, 5810.

33) Hamelin, A., in "Modern Aspects of Electrochemistry", Vol. 16, Conway, B.E., While, R.E., and Bockris, J.O'M., eds., Plenum Press, New York, 1985, Chapter 1.

34) Edens, G.J., unpublished observations.

35) An older overview of anion-induced cation adsorption is given in: Anson, F.C., Acc. Chem. Res., 1975, 8, 400.

36) Elliott, C.M. and Murray, R.W., J. Am. Chem. Soc., 1974, 96, 3321.

37) Electrosorption valency values close to -1.0 for iodide on Au(111) have been obtained by a thermodynamic analysis of C_d-E data.[34]

38) Gao, P. and Weaver, M.J., J. Phys. Chem., 1986, 90, 4057.

FIGURE CAPTIONS

Fig 1

Cyclic voltammograms at 50 mV s^{-1} for ordered Au(110) in 45 mM MClO$_4$ + 5 mM MI, where M$^+$ is A) K$^+$ and B) Cs$^+$. Symbols mark various phase transitions examined here (see text). Inset (C) shows cyclic voltammograms recorded over narrow potential range corresponding to adlayer I/II transition, at 50 mV s^{-1} (upper) and 5 mV s^{-1} (lower) (latter has 10-fold expanded current axis).

Fig 2

"Composite-domain" atomic-resolution STM image showing iodine adlayer I-substrate registry on Au(110) in 10 mM KI. Electrode potential was stepped from −0.35 V to −0.2 V one-third along the upward-rastered data acquisition.

Fig 3

A) Atomic resolution image of iodine adlayer I on Au(110) at −0.1 V. B) Close up of portion of A.

Fig 4

A,B) Schematic ball-model structures of iodine adlayers I and II considered here.

Fig 5

A) "Composite-domain" STM image showing iodine adlayer II-substrate registry on Au(110). Potential was stepped from −0.45 V to 0.1 V during upward-rastered image acquisition. B) "Composite-domain" image showing iodine adlayer I→II conversion during slow (5 mV s^{-1}) potential sweep from −0.02 to 0.05 V during upward-rastered data acquisition. D) Similar to C, but showing reverse adlayer II→I conversion, for 5 mV s^{-1} potential sweep from 0 to −0.08 V during downward-rastered data acquisition.

Fig 6

A) Large-scale structural changes appearing on Au(110) in 10 mM KI upon holding at 0.2 V for 2 min. B) Close-up atomic-resolution image of pair of iodine "strings", as seen in A, overlaid on (3 × 2)-I⁻ adlayer.

Fig 7

Sequence of STM images showing Au(110) long-range restructuring occurring in 10 mM KI at high potentials. A) Large-scale image at −0.4 V, showing semi-circular terrace regions. B) Similar region as A, b' 2 min after increasing potential to 0.1 V. C) Large-scale image obtained at 0.25 V, showing marked alterations in terrace-edge morphology. D) Same region as in C, but after holding at 0.35 V for 15 min. E) Atomic-resolution close up of restructured Au(110), showing string-channel morphology covered by (3 × 2)-I⁻ adlayer. F) Multilayer iodine film formed on Au(110) after onset of solution iodide electrooxidation at ca 0.45 V.

Fig 8

Sequence of potentiodynamic STM images of Au(110) in 10 mM KI during 10 mV s⁻¹ potential excursion from −0.45 to −0.8 V and return, showing formation and removal of (1 × 3) reconstruction. A) Upward-rastered image, while potential was swept from −0.6 to −0.8 V. B) Downward-rastered, −0.8 to −0.84 V and return sweep to −0.68 V. C) Upward-rastered, −0.68 to −0.48 V. D) Image obtained upon return to −0.45 V.

Fig 9

Similar to Fig 8, but for Au(110) in 10 mM CsI, showing resolvable stages of potential-induced reconstruction during 5 mV s⁻¹ potential excursion from −0.45 to −0.95 V. A) Upward-rastered image, while potential was swept from −0.55 to −0.65 V. B) Downward-rastered, −0.65 to −0.75 V. C) Upward-rastered, −0.75 to −0.85 V. D) Downward-rastered, −0.85 to −0.95 V.

Fig 10

A-C) Atomic-resolution STM images, showing structure of ordered mixed cesium-iodide adlayer formed on Au(110) in 10 mM CsI. A) "Composite-domain" image showing adlayer-substrate registry, created by stepping potential from −0.3 to −0.5 V during upward-rastered data acquisition. B,C) Images showing two commonly observed patterns. D) Suggested ball-model structural model.

FIG 1

FIG 2

B

A

FIG 3

Au (110)-I (0 13) unit cell
(-3 1)

FIG 4A

Au(110)-I (3 x 2) unit cell
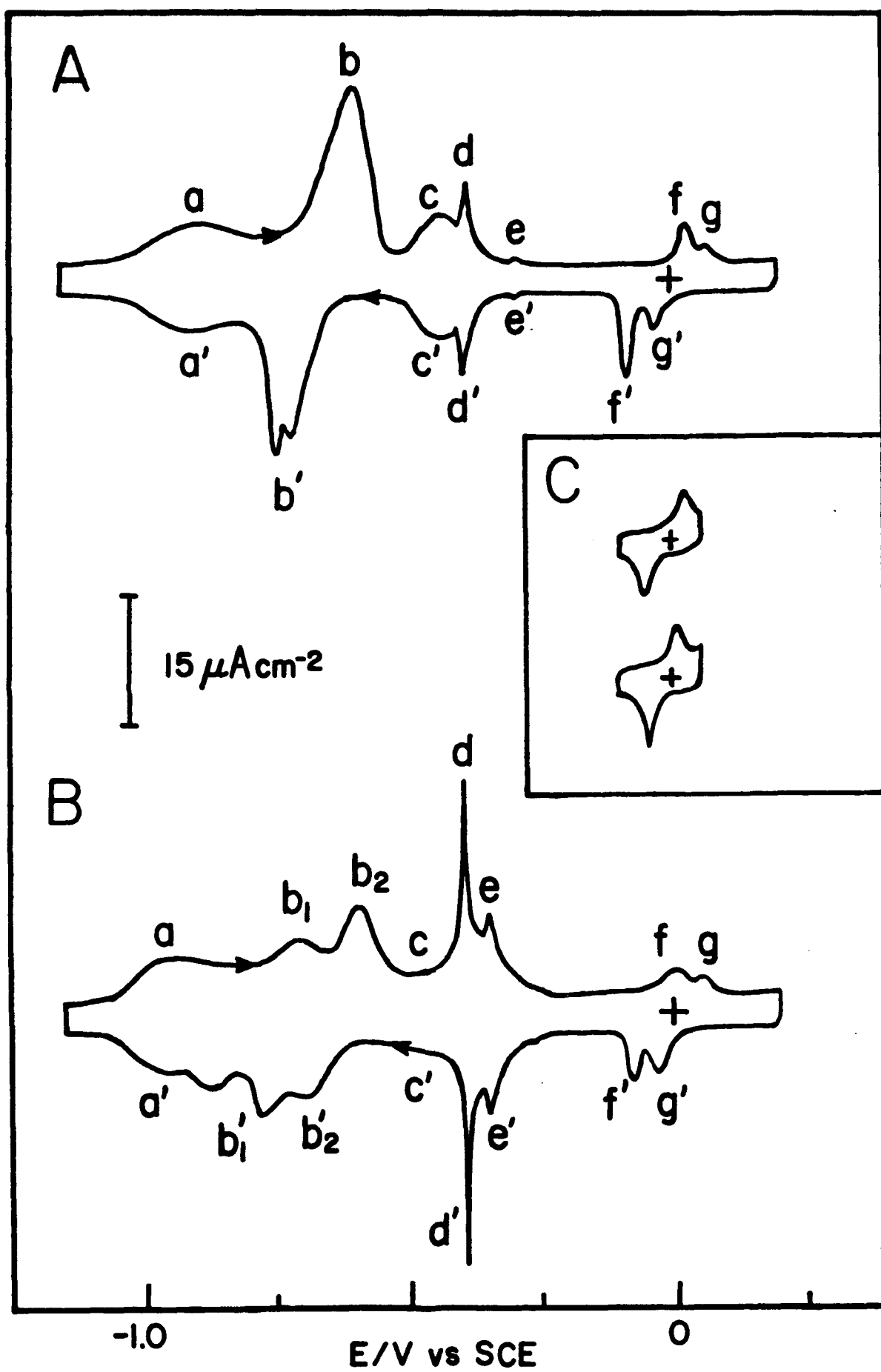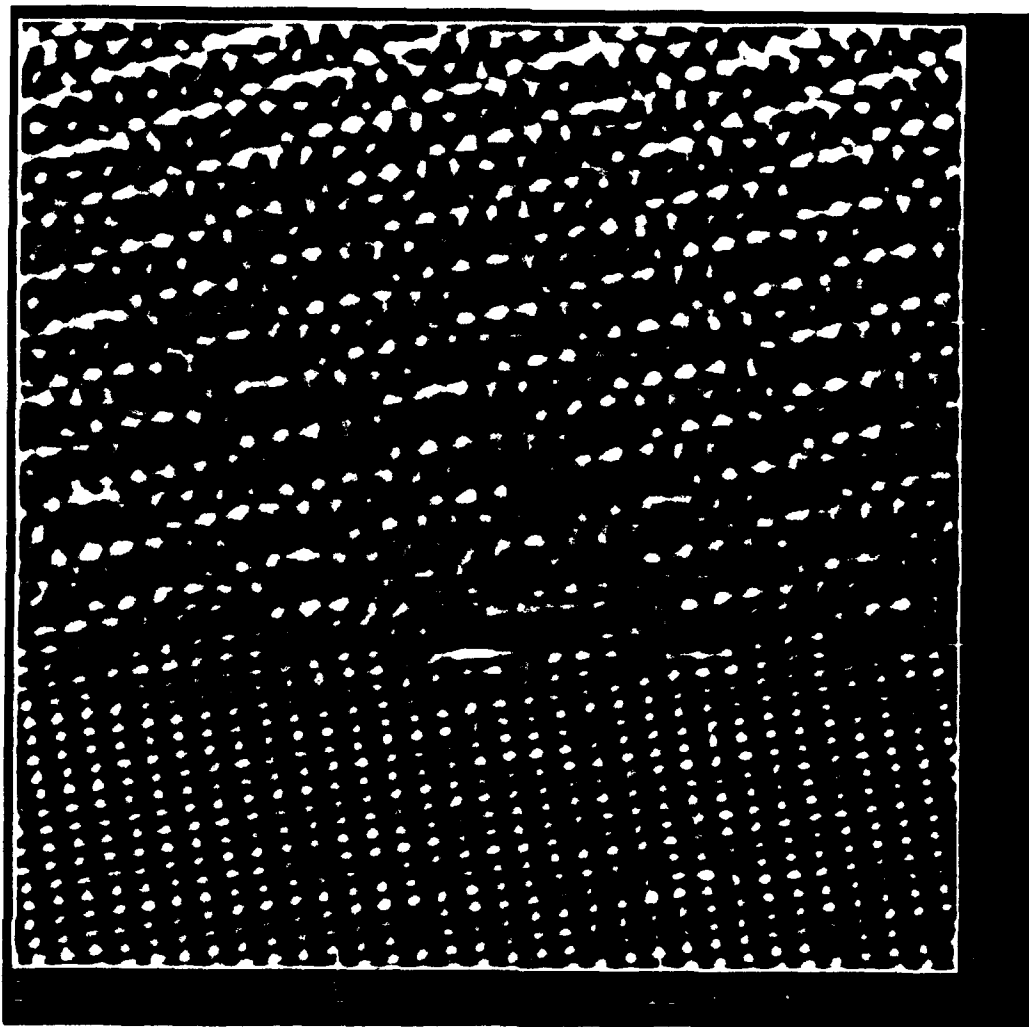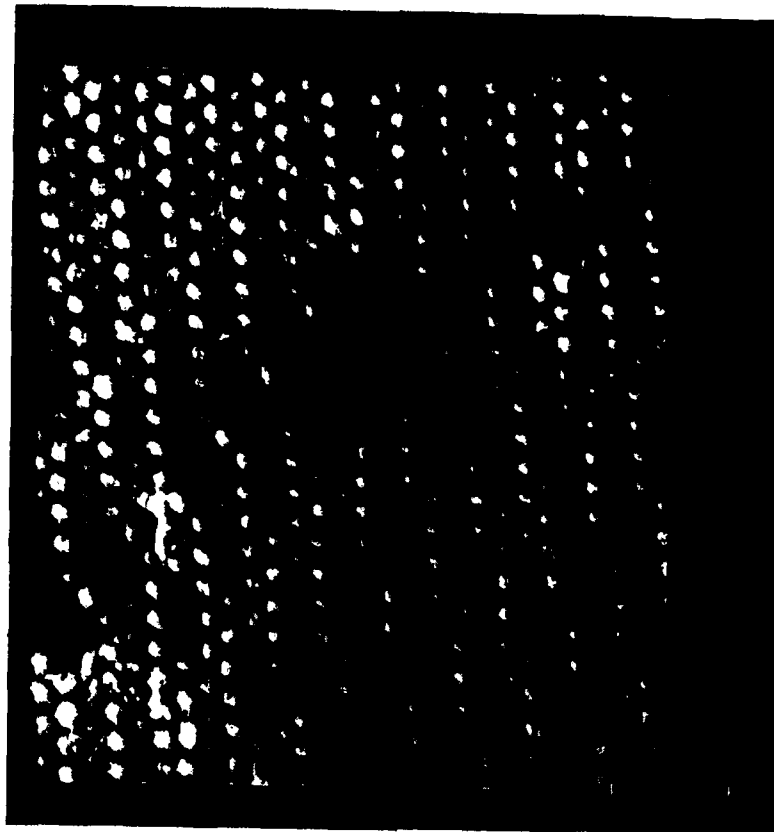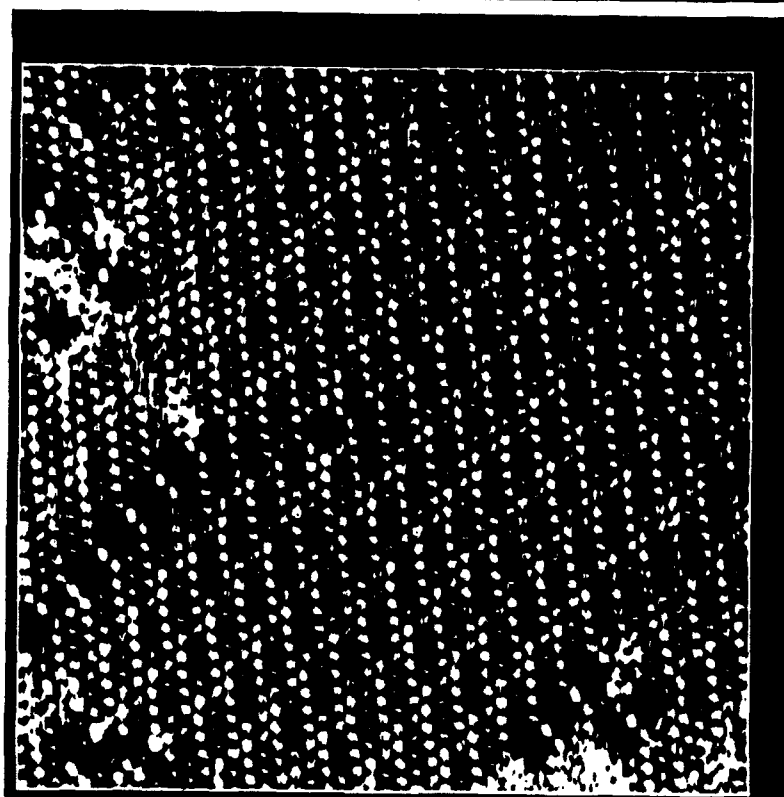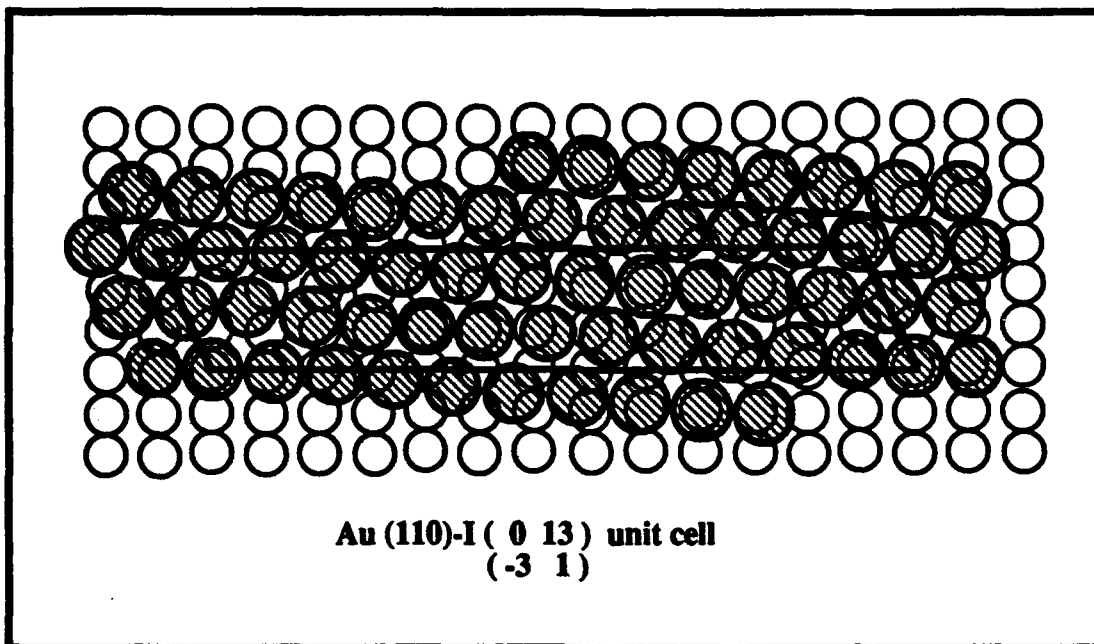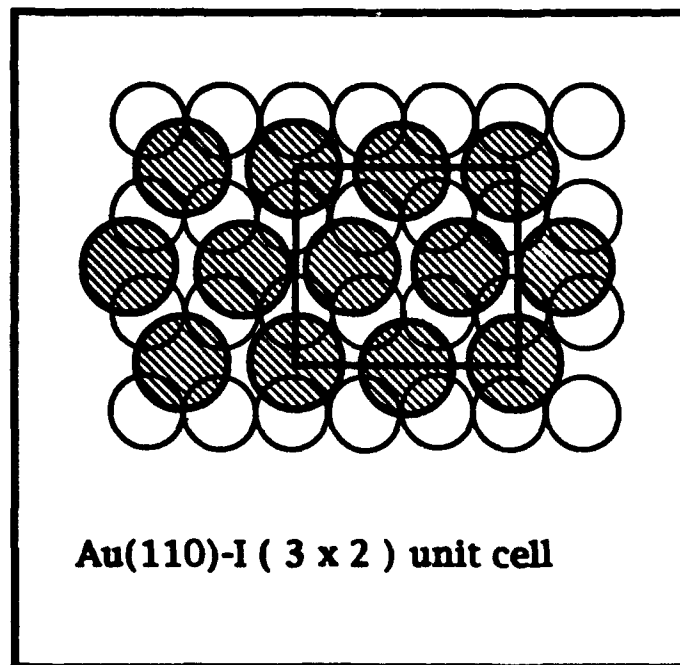
FIG 4B
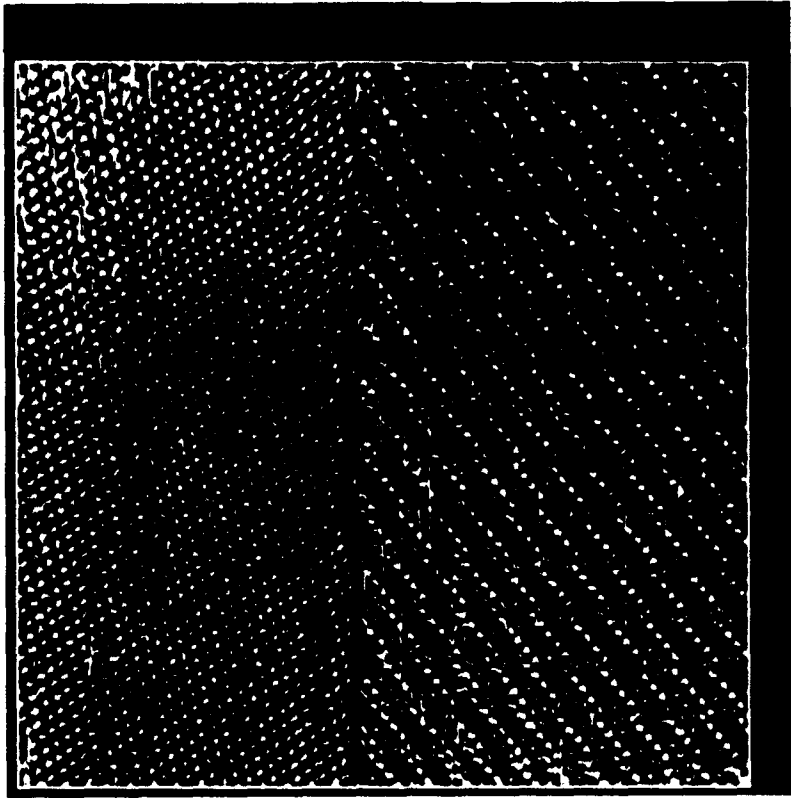
B
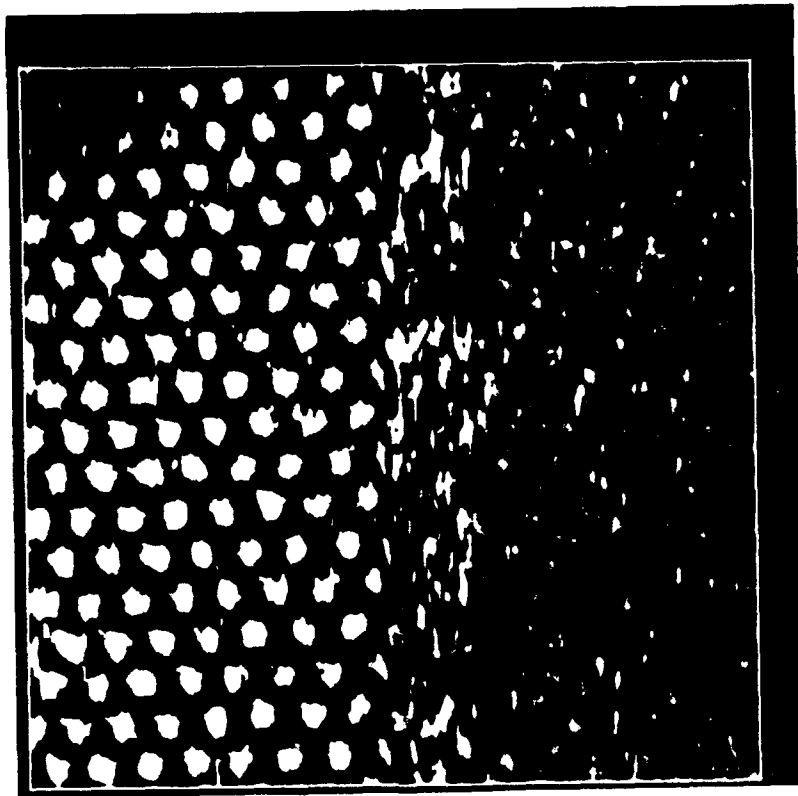
A
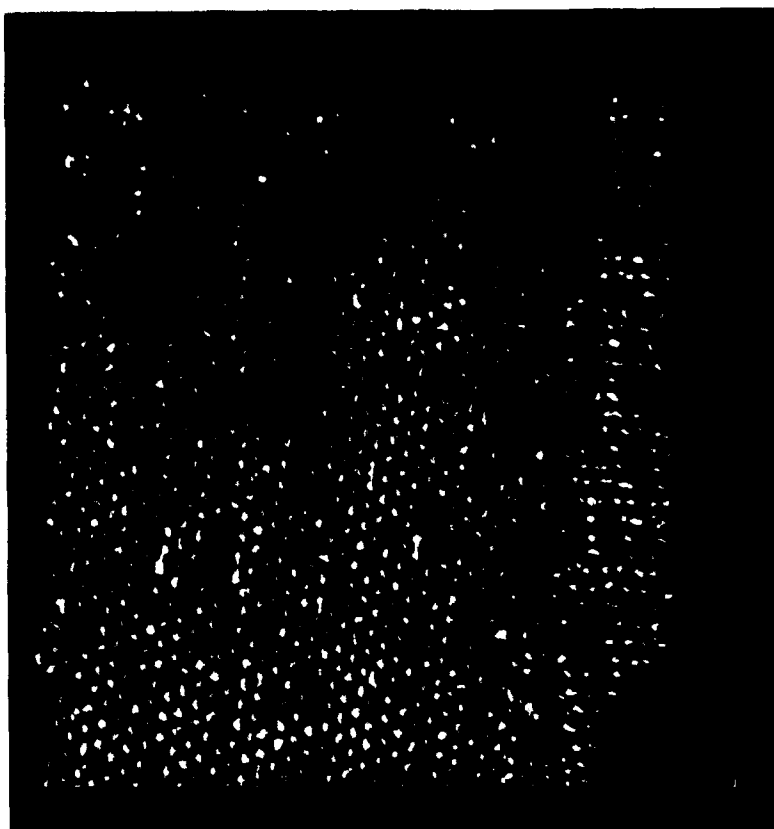
FIG 5

D
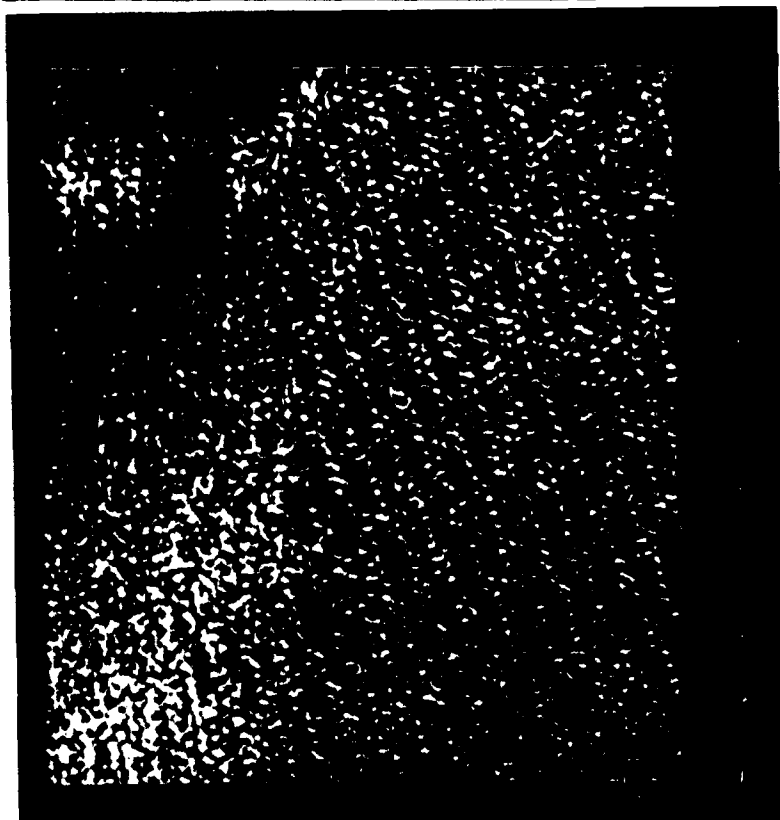
C

FIG 5 (CONTD)

B

A

FIG 6
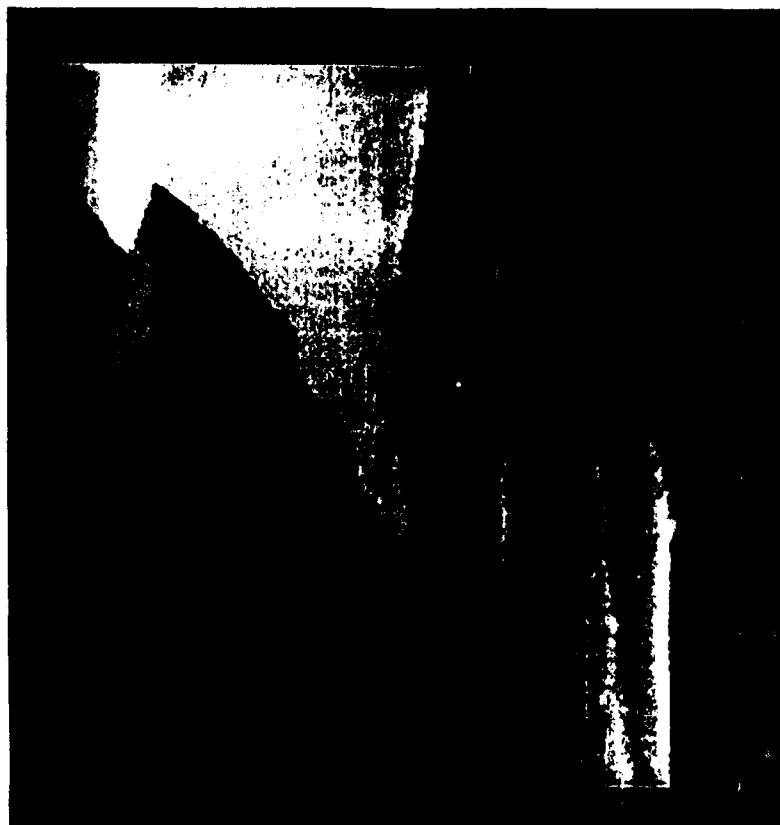
B
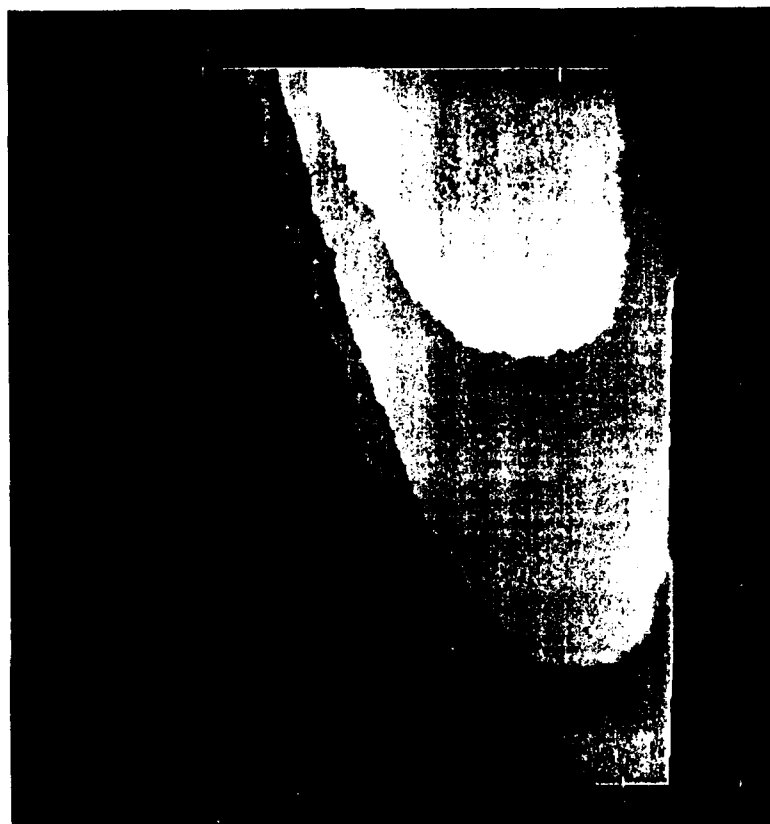
A

FIG 7
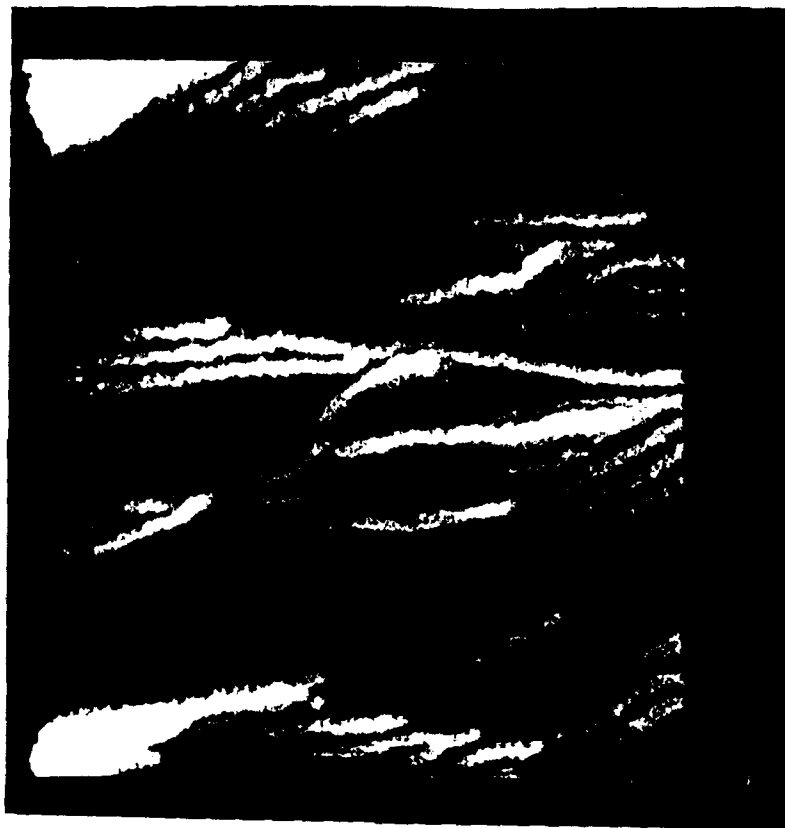
A

C

FIG 7 (CONTD)

F

E

FIG 7 (CONTD)

B

A

FIG 8

A
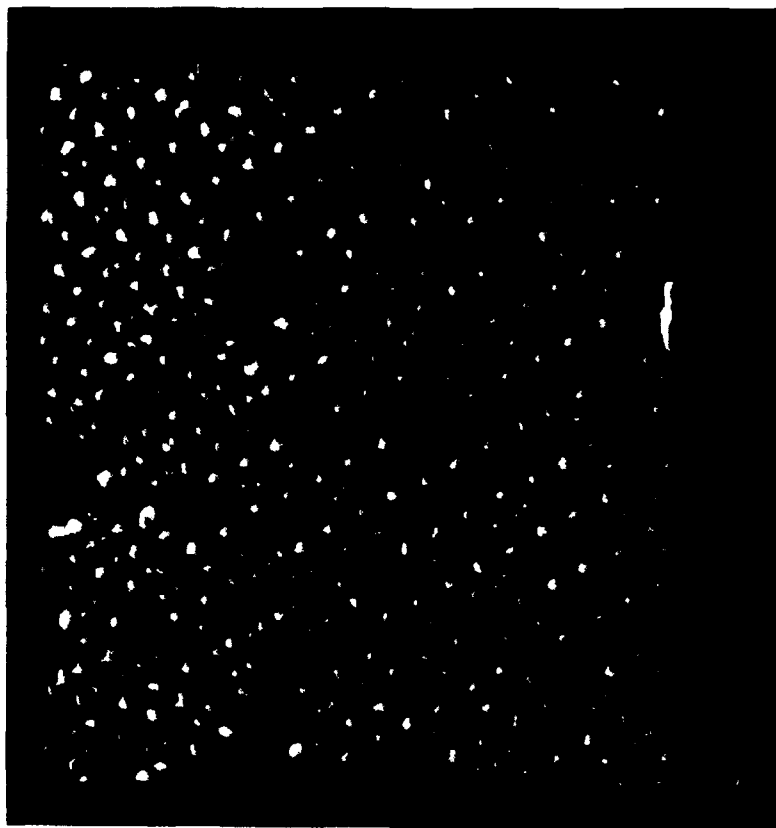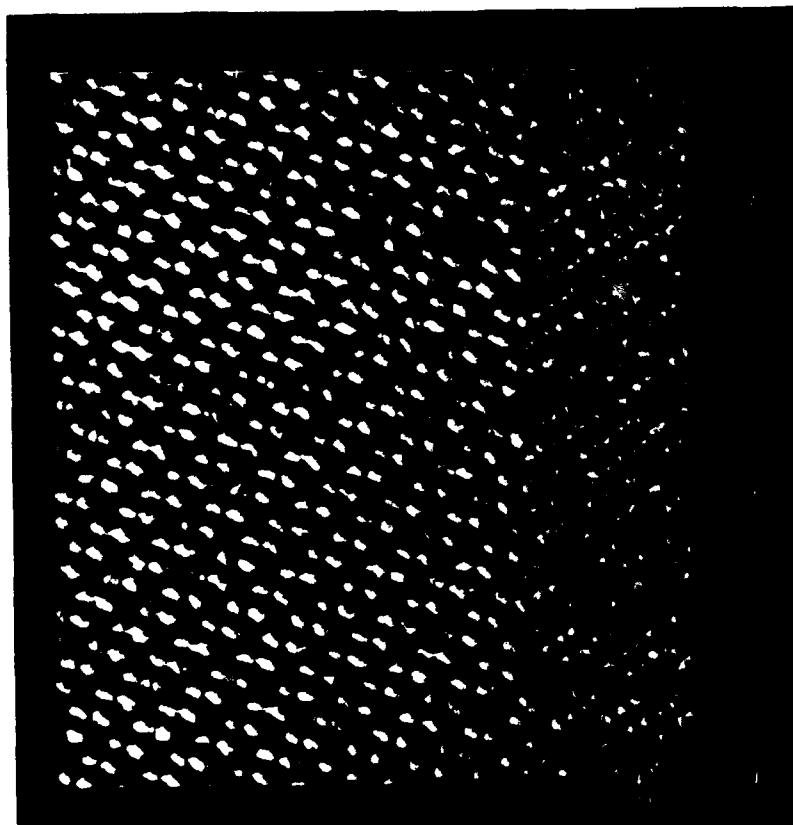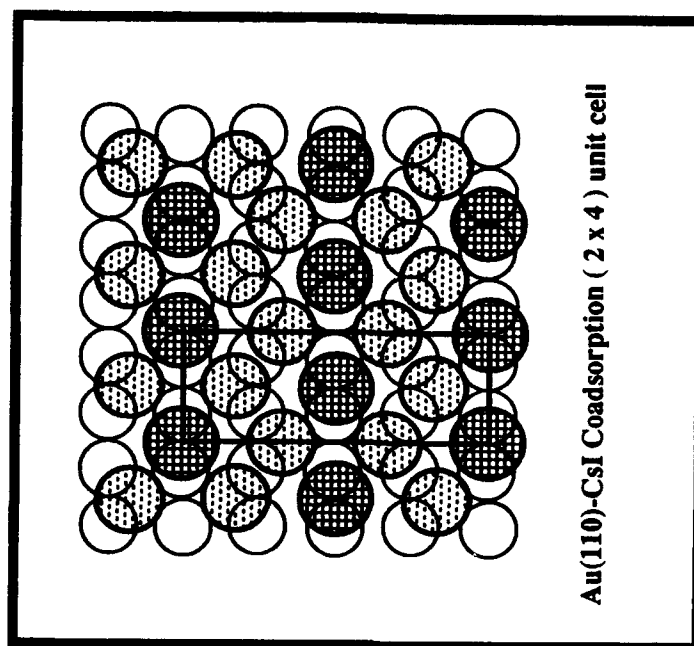
C

FIG 8 (CONTD)

B

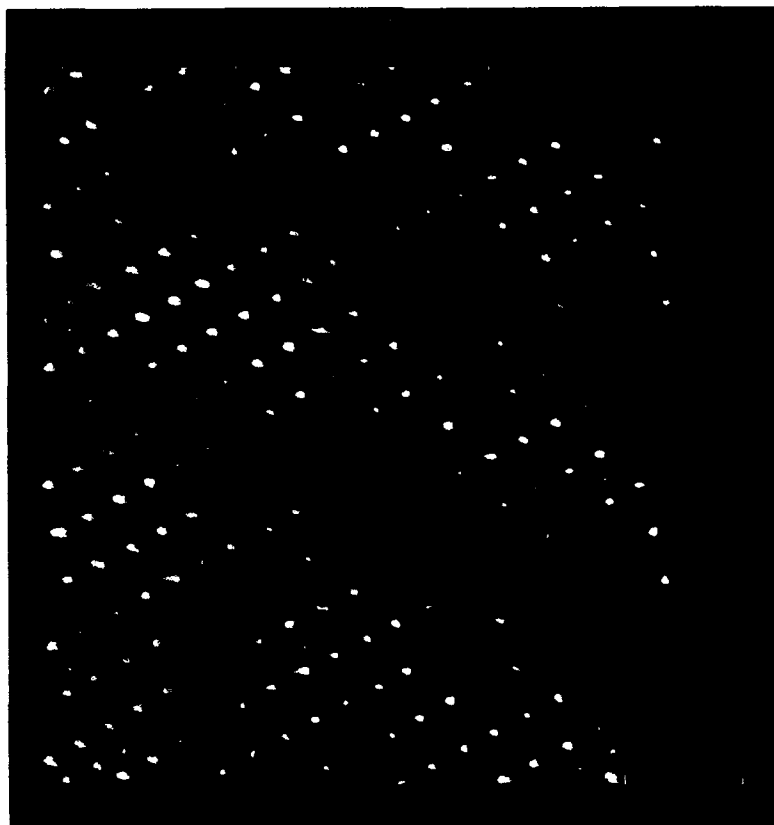A

FIG 9

D

C

FIG 9 (CONT'D)

B

A

FIG 10

Au(110)-CsI Coadsorption (2 x 4) unit cell

A

C

FIG 10 (CONT'D)